Domain growth of Dy_2O_3 buffer layers on $SrTiO_3$

A. Catana[a] and J-P. Locquet
IBM Research Division, Zurich Research Laboratory, 8803 Rüschlikon, Switzerland

(Received 17 August 1992; accepted 29 January 1993)

Dy_2O_3 layers have been grown on $SrTiO_3$ by molecular beam epitaxy. X-ray and electron diffraction patterns clearly show that Dy_2O_3 grows epitaxially on $SrTiO_3$ with {100} planes parallel to the substrate surface. Transmission electron microscopy reveals that the Dy_2O_3 film breaks up into small domains (10–40 nm). This leads to the formation of terraces which limits the structural perfection of thin overgrown $DyBa_2Cu_3O_7$ by introducing steps and small misorientations (within 3°). The resulting surface corrugation does not preclude the growth of epitaxial c-axis $DyBa_2Cu_3O_7$ films with a T_{c0} of 86 K. Crystallographic analysis and image calculations show that the domain growth of Dy_2O_3 is associated with the formation of 90° rotation twins.

I. INTRODUCTION

The properties of thin superconducting layers (a few unit cells thick) are strongly influenced by the chemical and structural properties of the substrate. Thus, there is an effort toward growth of compatible oxide buffer layers on most commonly used substrates such as $SrTiO_3$, MgO, and Si. This interest is partly driven by the development of tunnel junctions and passive or active devices. Successful applications of buffer layers have been reported for materials that are structurally and chemically very similar to the desired superconductor. For the $REBa_2Cu_3O_7$ (REBCO: RE = rare earth) family, $PrBa_2Cu_3O_7$ (Ref. 1) and $La_1Ba_2Cu_3O_7$ (Ref. 2) have been used as a buffer layer and a protection layer for single thin films as well as multilayers[3] on MgO or $SrTiO_3$. Other superconductor/buffer layer pairs exist such as $(La,Sr)_2CuO_4/Sm_2CuO_4$ (Ref. 4) and $Bi_2Sr_2Ca_{0.85}Y_{0.15}Cu_2O_8/Bi_2Sr_2Ca_{0.5}Y_{0.5}Cu_2O_8$.[5] In general, such buffer layers have the advantage of low chemical reactivity with the superconductor layer and have a similar surface symmetry. Another approach is to use oxides with structures that are identical to that of the commonly used substrate oxides. Examples for this include $SrTiO_3$,[6] MgO,[7] and Y-stabilized ZrO_2.[8]

A third group includes the RE oxides (RE_2O_3),[9] in particular Y_2O_3 and Dy_2O_3, with a low dielectric constant and a lattice mismatch with respect to YBCO or DBCO, which is comparable to that provided by $SrTiO_3$. They were used in sandwich structures to demonstrate Josephson supercurrents[10] or to measure tunneling characteristics.[11–13] For the fabrication of tunnel junctions it is important to grow planar, pinhole-free buffer layers with abrupt interfaces. To reach these goals a better understanding and control of the growth mechanisms is necessary, which in turn requires a detailed structural analysis of both buffer and DBCO layers. In particular, we need to understand the influence of the buffer layer structure on the overgrown superconducting layer and the resulting interfaces.

II. EXPERIMENTAL PROCEDURE

In this paper we report on the growth of epitaxial Dy_2O_3 on $SrTiO_3$ and on the growth of DBCO on top of the Dy_2O_3 layer, with particular emphasis on the domain structure of Dy_2O_3. The growth technique used is molecular beam deposition; Cu, Ba, and Dy are evaporated from standard effusion cells in an oxygen background pressure generated by an efficient rf plasma source which delivers a flow of atomic oxygen onto the substrate.[14] Typical growth conditions were a substrate temperature of 750 °C and an oxygen background pressure of 1×10^{-5} Torr. This pressure was used during both growth and cooling. Structural analysis of the film surface is performed by reflection high-energy electron diffraction (RHEED).

Transmission electron microscopy (TEM) samples were prepared for both planar and cross-sectional investigations by mechanical polishing and ion-milling with liquid nitrogen cooling. The observations were performed on a JEOL JEM-2010 operating at 200 kV. Image calculations were performed using the Bloch wave algorithm of the EMS software package developed by Stadelmann.[15]

III. RESULTS AND DISCUSSION

Dy_2O_3 has body-centered cubic structure (a = 1.06 nm) and belongs to the space group $Ia\bar{3}$. Although cubic, it has neither fourfold symmetry axes nor mirror planes, in contrast to the $SrTiO_3$ substrate (Fig. 1).

[a]Present address: Prospectives et Recherche, EPFL, 1015 Lausanne, Switzerland.

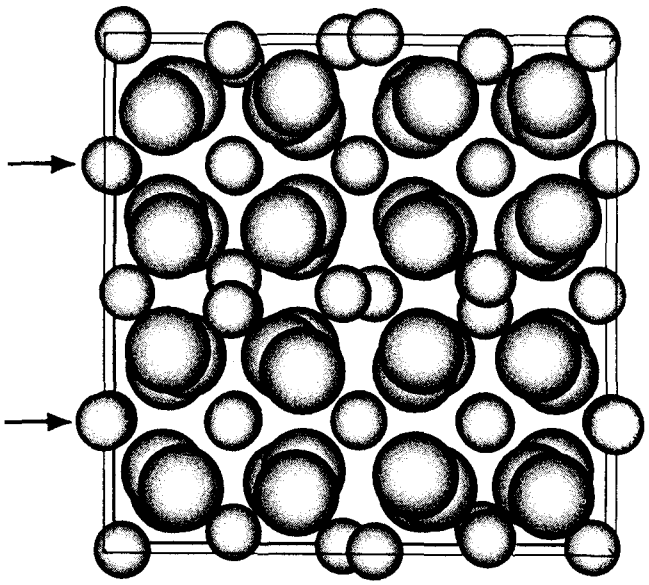

FIG. 1. [100] projection of the Dy_2O_3 unit cell (Dy: small circles, O: large circles). Arrows indicate the ordering of Dy single chains parallel to (001) planes. Such chains appear ordered parallel to (100) and (010) when projected along [010] and [001], respectively.

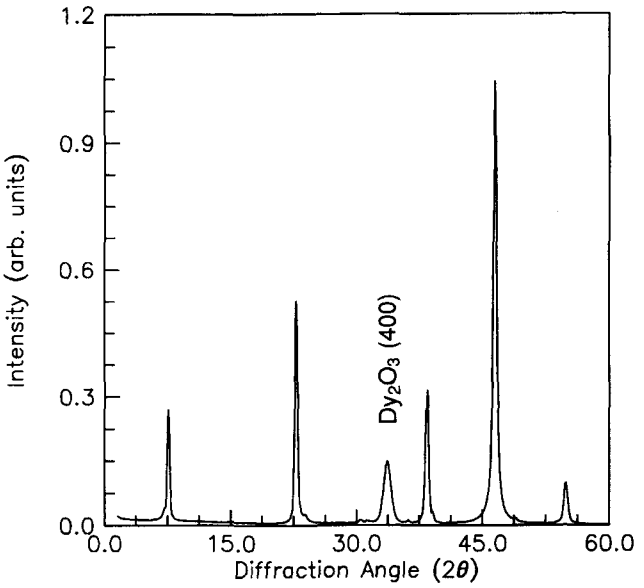

FIG. 3. X-ray diffraction pattern of the bilayer structure DBCO/Dy_2O_3 grown on $SrTiO_3$ (001).

Epitaxial Dy_2O_3 layers as thin as 7.5 nm are grown on $SrTiO_3$, and subsequently superconducting DBCO (20 nm) films with transition temperatures of 86 K are deposited (Fig. 2). The x-ray diffraction pattern in Fig. 3 provides a first insight into the epitaxial growth of Dy_2O_3 with its 100 planes parallel to the substrate surface, as well as into the structure of the overlying c-axis-oriented DBCO. The Dy_2O_3 peak corresponding to the (400) reflections is approximately three times as broad as that of DBCO. This is consistent with the DBCO/Dy_2O_3 thickness. The other peaks correspond to the (001) reflections of DBCO. Electron diffraction and TEM (Fig. 4) clarify the in-plane orientation relationship between $SrTiO_3$ and the bilayer system: ⟨110⟩ $SrTiO_3$ ‖ ⟨100⟩ Dy_2O_3 ‖ ⟨110⟩ DBCO. Along these axes the mismatch between nearly coincident supercells in the interface plane is 3.3% and 2.2% for $SrTiO_3$ and DBCO, respectively. This mutual orientation is in agreement with recently reported results.[11,12] Planar views show that 90° boundaries split the oxide film into domains [Fig. 4(a)]. TEM observations at higher magnifications show that the resulting boundary regions are disordered within 1–2 monolayers (Fig. 5). As one crosses such boundaries, slight misorientations of the lattice are occasionally observed. To gain a better understanding of the structure at the resulting interfaces, cross-sectional observations are needed. Since the domain boundaries lie along {100} Dy_2O_3 planes, their detection and proper imaging require the electron beam to be parallel to ⟨100⟩ Dy_2O_3, and in turn to ⟨110⟩ $SrTiO_3$. Otherwise, strong overlap will occur among the various Dy_2O_3 domains, which hides the real structure of the buffer film and of its interfaces.

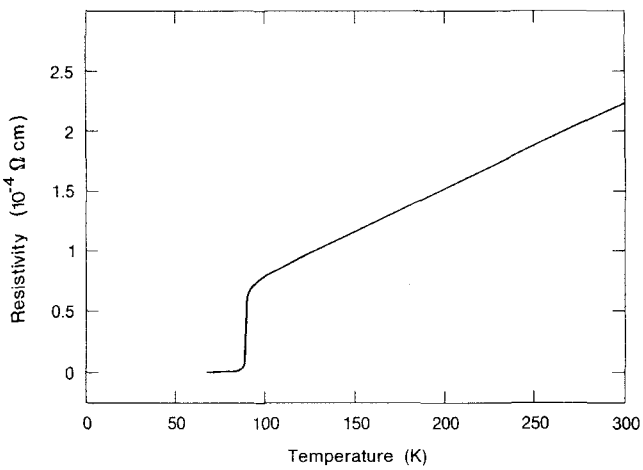

FIG. 2. Resistance measurement of the bilayer film (T_c = 86 K). From Ref. 14.

Figure 6 is a bright-field micrograph of the bilayer structure ($SrTiO_3$/Dy_2O_3/DBCO) displaying the layered structure of DBCO, as well as the domain growth of Dy_2O_3. Some domains are slightly misoriented with respect to the electron-beam axis (they appear brighter in the image), indicating that small misalignments occur during growth. Contrast modulation at the $SrTiO_3$/Dy_2O_3 interface indicates the presence of strain, which is related to the lattice mismatch and domain growth of Dy_2O_3. Owing to the misorientations between

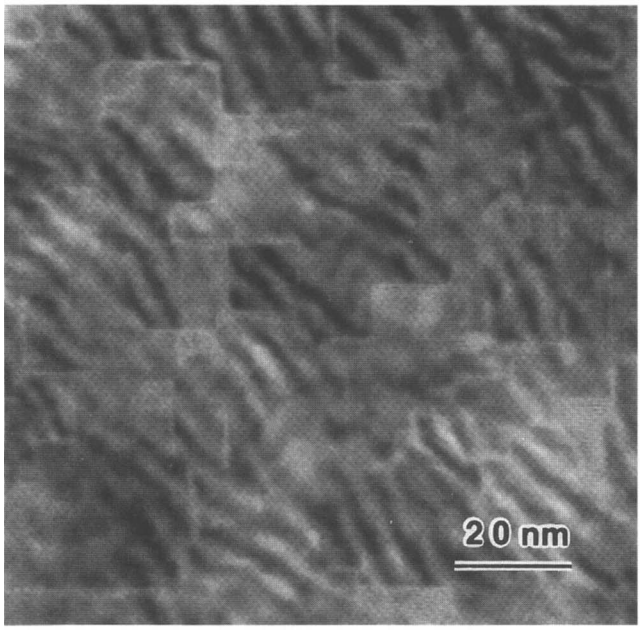

(a)

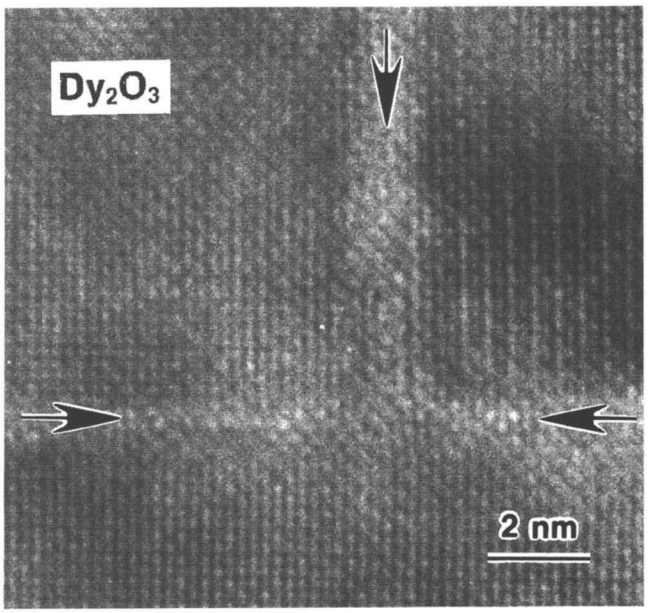

FIG. 5. Planar-view HREM of disordered Dy_2O_3 domain boundaries.

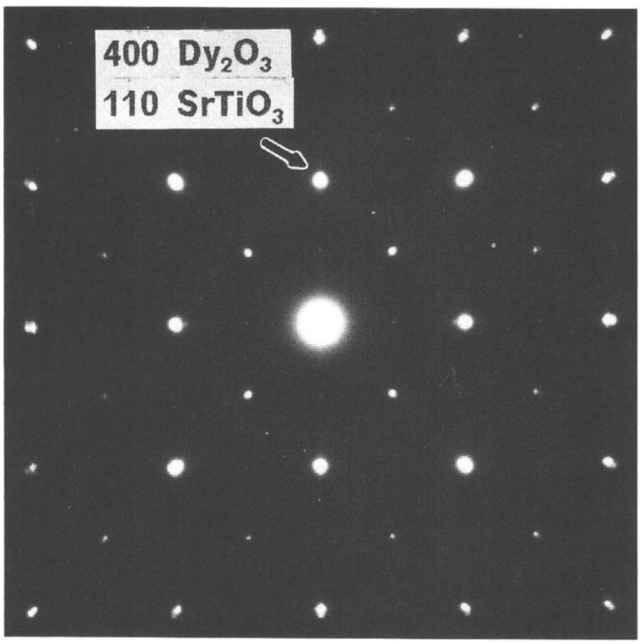

(b)

FIG. 4. (a) Planar view of Dy_2O_3 domain boundaries lying along {100} planes as indicated by electron diffraction (b). The superimposed moiré pattern results from the overlap between $SrTiO_3$, Dy_2O_3, and DBCO.

the different domains and their thicknesses, terraces are formed at the Dy_2O_3 surface, which preclude a perfectly planar growth of DBCO layers. These follow the surface profile, thus leading to a slightly undulated film, as observed in Fig. 6. The maximum angular misorientation between adjacent domains or between the domains and substrate is about 3°, which is consistent with recently reported results on low-angle grain boundaries in bulk Dy_2O_3.[16] This feature is confirmed by high-resolution observations such as those displayed in Fig. 7. However, neither dislocations nor strain can be observed at the Dy_2O_3/DBCO interface. The bilayer structure and typical boundaries between Dy_2O_3 domains are imaged at high resolution in Fig. 8. Both the $SrTiO_3/Dy_2O_3$ and the Dy_2O_3/DBCO interfaces are abrupt. Locally, the upper interface shows steps of about 1.1 nm [Fig. 8(b)]. This height can easily be accommodated by DBCO since it closely matches the c-axis of the unit cell. As a result, there are no strong distortions at the DBCO/Dy_2O_3 interface in this case. Interfacial steps corresponding to nonintegral numbers of unit cells may also exist—such a situation would then be related to stronger interfacial distortions of the DBCO layers. The domain structure is related to the breaking of the fourfold symmetry of the substrate by the Dy_2O_3 grown. The resulting domains are characterized by different ordering directions of Dy planes (Fig. 1) with respect to the substrate and should therefore be observable in high-resolution electron microscopy (HREM) micrographs. Indeed, the ordering of Dy equally spaced chains appears either parallel or normal to the surface. As growth proceeds, the rotation twins join, leading to the formation of boundaries. The experimental and calculated HREM images shown in Fig. 9 reveal that the ordering of Dy atoms changes as one crosses the domain boundary. On one side (domain A) the ordering is normal to the substrate surface (as in Fig. 7); on the other (domain B) it is parallel to it.

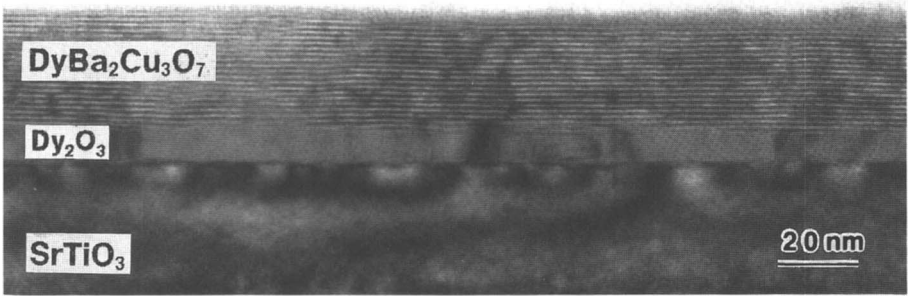

FIG. 6. Cross-sectional bright-field micrograph recorded along ⟨110⟩ $SrTiO_3$ shows the domain structure of the buffer layer. The surface of the DBCO layer is planar within one unit cell. Roughness at the Dy_2O_3/DBCO interface and strain-induced contrast modulations at the $SrTiO_3/Dy_2O_3$ are clearly observed.

IV. SUMMARY

In summary, epitaxial Dy_2O_3/DBCO structures have been grown on $SrTiO_3$ substrates with transition temperatures of 86 K. The DBCO is found to grow exclusively with c-axis orientation. Detailed structural analysis, particularly based on HREM and image calculations, reveals the domain growth of Dy_2O_3: observations along ⟨110⟩ $SrTiO_3$ clearly show 10–40 nm domains oriented such that ⟨100⟩ Dy_2O_3 ‖ ⟨110⟩ $SrTiO_3$ and {100} Dy_2O_3 ‖ {100} $SrTiO_3$. The interface is abrupt but highly strained. Small misorientations between the domains with respect to the substrate, as well as slight thickness variations, induce roughness at the Dy_2O_3/DBCO interface. Atomic-scale investigations show that the domain growth of Dy_2O_3 is connected with the formation of 90° rotated domains.

ACKNOWLEDGMENTS

We gratefully acknowledge stimulating discussions with J. G. Bednorz and T. Schneider as well as the valuable support of E. Mächler and R. F. Broom, and the financial support of the Swiss National Science Foundation.

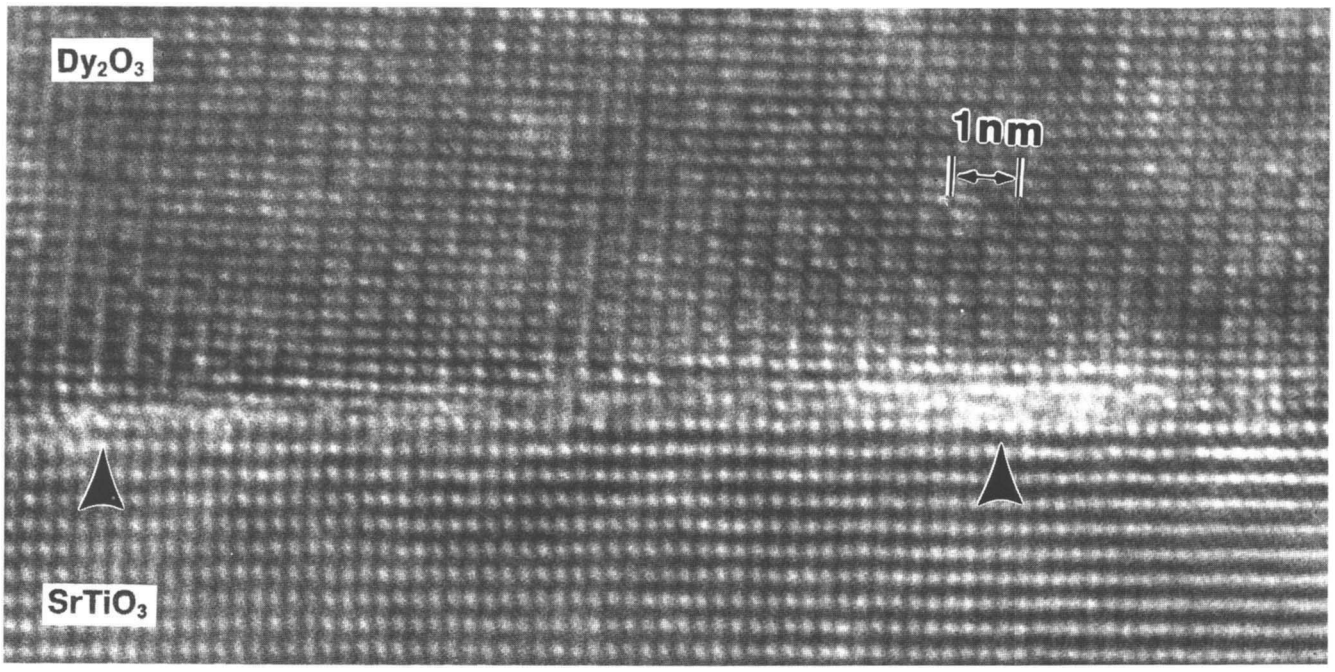

FIG. 7. Inclined Dy_2O_3 domain with respect to the $SrTiO_3$ substrate. Arrows indicate regions of misfit.

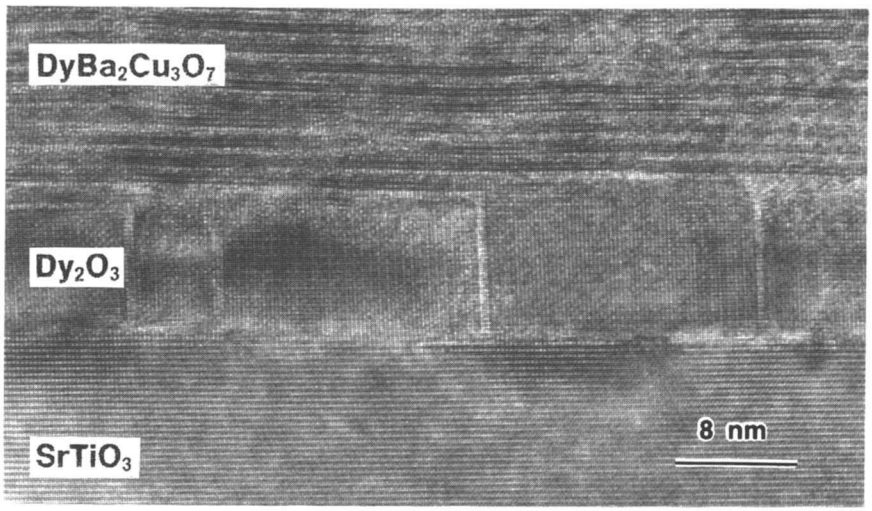

(a)

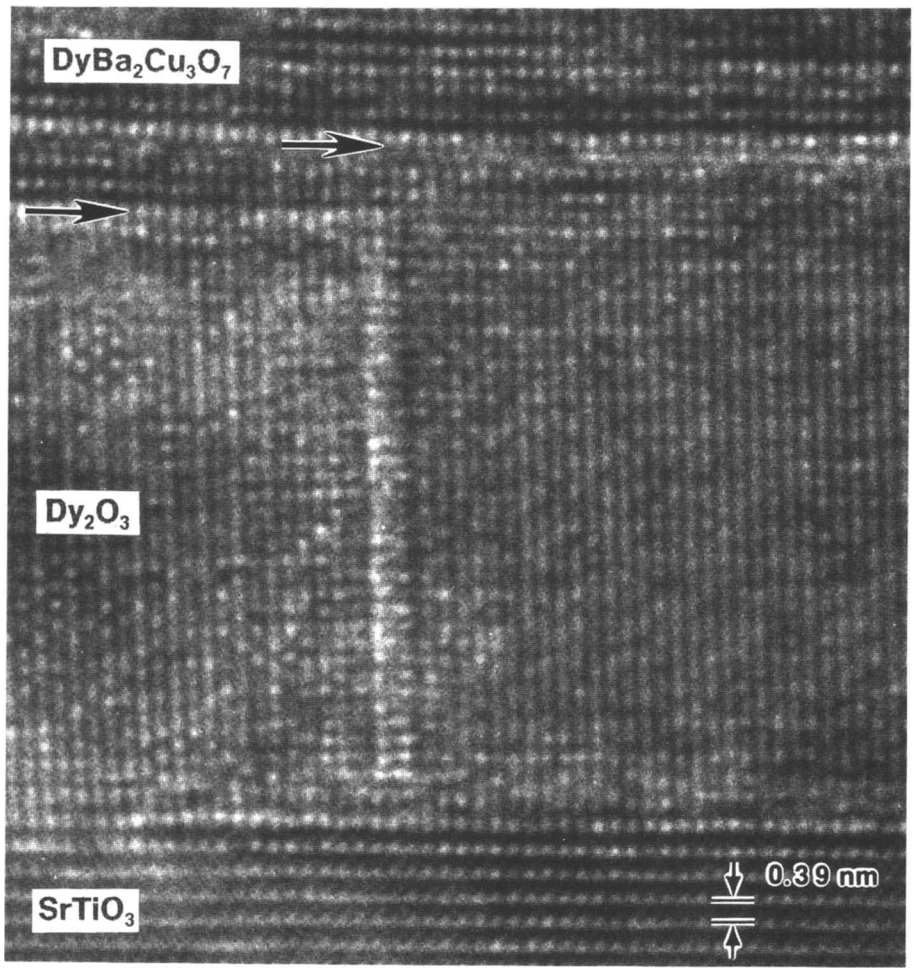

(b)

FIG. 8. (a) Cross-sectional lattice image of the bilayer structure. (b) High-magnification image of a boundary between two Dy_2O_3 domains. The arrow indicates an interface step of about 1.1 nm.

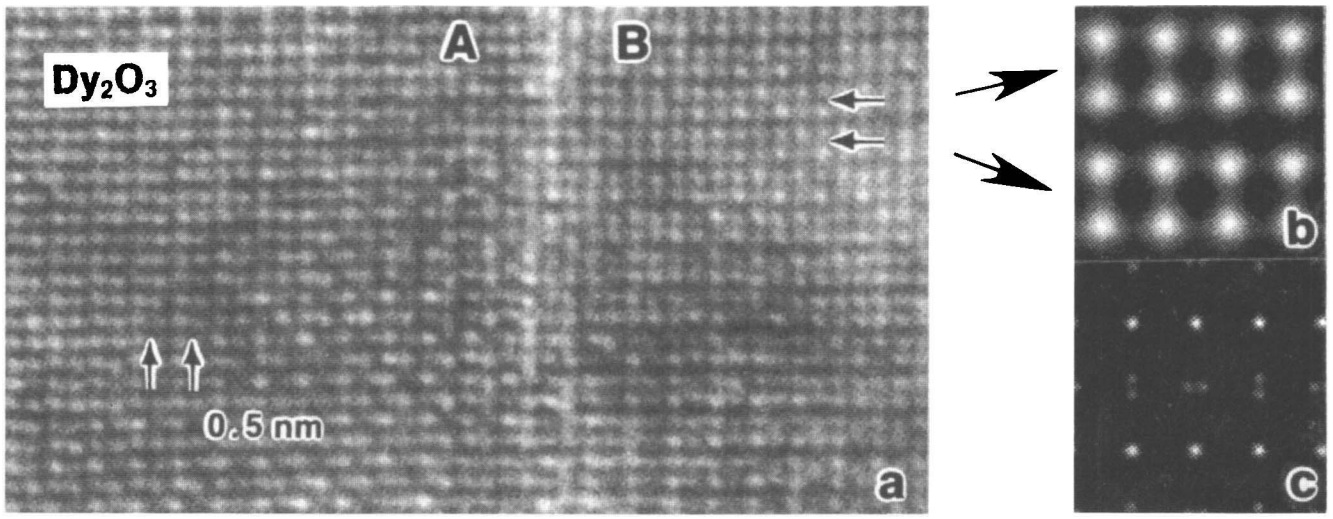

FIG. 9. (a) Cross-sectional lattice image at a boundary that separates two domains (A, B) related by a 90° rotation around [100]. In domain A, Dy single chains are ordered in planes normal to the substrate surface, whereas in B they are parallel to the surface, as indicated by periodic contrast modulations (arrows) in both experimental and calculated images (b). (c) shows the projected atomic potential: bright dots represent single chains of Dy atoms (see Fig. 1). The microscope parameters used for the calculation are spherical aberration coefficient = 1.0 mm, spread of focus = 8 nm, beam semiconvergence = 0.8 mrad, defocus = 54 nm. Sample thickness = 6 nm.

REFERENCES

1. T. Terashima, Y. Bando, K. Iijima, K. Yamamoto, K. Kirata, K. Hayashi, K. Kamigaki, and H. Terauchi, Phys. Rev. Lett. **65**, 2684 (1990).
2. O. Nakamura, I. N. Chan, J. Guimpel, and Ivan K. Schuller, Appl. Phys. Lett. **59**, 1240 (1991).
3. J. M. Triscone, Ø. Fisher, O. Brunner, L. Antognazza, A. D. Kent, and M. G. Karkut, Phys. Rev. Lett. **64**, 804 (1990).
4. H. Tabata, T. Kawai, and S. Kawai, Appl. Phys. Lett. **58**, 1443 (1991).
5. M. Kanai, T. Kawai, and S. Kawai, Appl. Phys. Lett. **57**, 198 (1990).
6. J. Mannhart, D. G. Schlom, J. G. Bednorz, and K. A. Müller, Phys. Rev. Lett. **67**, 2099 (1991).
7. J-W. Lee, M. Migliuolo, A. K. Stamper, D. W. Greve, D. E. Laughlin, and T. E. Schlesinger, Appl. Phys. Lett. **66**, 4886 (1989).
8. S. Witanachchi, S. Patel, D. T. Schaw, and H. S. Kwok, Appl. Phys. Lett. **55**, 295 (1989).
9. J. A. Edwards, N. G. Chew, S. W. Goodyear, J. S. Satchell, S. E. Blenkinsop, and R. G. Humphryes, J. Less-Comm. Met. **164**, 414 (1990).
10. M. G. Blamire, G. W. Morris, R. E. Somekh, and J. E. Evetts, J. Phys. D **20**, 1330 (1987).
11. Q. Y. Ying, C. Hilbert, N. Kumar, D. Eichman, M. Thompson, H. Kroger, and D. M. Hwang, Appl. Phys. Lett. **59**, 3036 (1991).
12. K. M. Beauchamp, Y-J. Zhang, B. R. Johnson, R. K. Schultz, G. C. Spalding, M. Tsen, T. Wang, J. F. Evans, M. L. Mecartney, and A. M. Goldman, IEEE Trans. Magn. **27**, 3090 (1991).
13. K. Hirata, K. Yamamoto, K. Iijima, J. Takada, T. Terashima, Y. Bando, and H. Mazaki, Appl. Phys. Lett. **56**, 683 (1990).
14. J-P. Locquet and E. Mächler, J. Vac. Sci. Technol. A **10**, 3100 (1992).
15. P. Stadelmann, Ultramicroscopy **21**, 131 (1987).
16. A. Oishi, H. Teshima, K. Ohata, H. Izumi, S. Kawamoto, T. Morishita, and S. Tanaka, Appl. Phys. Lett. **59**, 1902 (1991).